

SPECIAL COLLECTION: GLASSES, MELTS, AND FLUIDS, AS TOOLS FOR UNDERSTANDING VOLCANIC PROCESSES AND HAZARDS

Melt inclusion CO₂ contents, pressures of olivine crystallization, and the problem of shrinkage bubbles‡

PAUL J. WALLACE^{1,*}, VADIM S. KAMENETSKY² AND PABLO CERVANTES^{3,†}

¹Department of Geological Sciences, University of Oregon, Eugene, Oregon 97403, U.S.A.

²School of Physical Sciences, University of Tasmania, Hobart, Tasmania 7001, Australia

³Department of Geology and Geophysics, Texas A&M University, College Station, Texas 77845, U.S.A.

ABSTRACT

The H₂O and CO₂ contents of melt inclusions can potentially be used to infer pressures of crystallization and inclusion entrapment because the solubility of mixed H₂O-CO₂ vapor has been determined experimentally for a wide range of melt compositions. However, melt inclusions commonly develop a shrinkage bubble during post-entrapment cooling and crystallization because these processes cause a pressure drop in the inclusion. This pressure drop causes a vapor bubble to nucleate, leading to exsolution of low-solubility CO₂ from the trapped melt. To investigate the loss of CO₂ into such bubbles, we experimentally heated large, naturally glassy melt inclusions in olivine (Fo contents of 88.1 ± 0.2) from a Mauna Loa picrite to rehomogenize the inclusions. Rapid heating to 1420 °C using a high-temperature heating stage dissolved the shrinkage bubbles into the melt. CO₂ contents measured by FTIR spectroscopy and recalculated for melt in equilibrium with the olivine host are 224–505 ppm (n = 11) for heated inclusions, much higher than the CO₂ contents of naturally quenched inclusions from the same sample (38–158 ppm; n = 8). Pressures of inclusion entrapment calculated from the H₂O and CO₂ data for the heated inclusions range from 0.5 to 1.1 kbar, indicating that Mg-rich olivine crystallized at very shallow depths beneath the surface of Mauna Loa. Our results indicate that 40–90% (average 75%) of the original CO₂ dissolved in the melt at the time of inclusion entrapment can be lost to the shrinkage bubble during post-entrapment cooling. We show that the computational method of Riker (2005), which predicts the pre-eruption shrinkage bubble size as a function of the difference between trapping temperature and pre-eruption temperature, successfully reproduces our experimental results. Our results demonstrate that the mass of CO₂ contained in shrinkage bubbles must be considered to accurately infer original pressures of crystallization for melt inclusions. However, the effect is expected to be smaller for more H₂O-rich melt inclusions than those studied here because the vapor bubble in such inclusions will have lower mole fractions of CO₂ than the low-H₂O inclusions in our study.

Keywords: Melt inclusions, volatiles, carbon dioxide, shrinkage bubble

INTRODUCTION

As magma ascends to the Earth's surface, dissolved volatiles are lost from the melt as a result of decompression because they have pressure-dependent solubility. This makes it difficult to investigate the volatile contents of magma by direct analysis of erupted material. Melt inclusions are small volumes of silicate melt that are trapped inside of phenocrysts at depth before eruption. Because the host crystal acts like a tiny pressure vessel, melt inclusions remain at higher pressure than the ambient melt surrounding the crystals as magma moves toward the surface and erupts. As a result, analysis of melt inclusions can potentially provide a record of magmatic conditions, including dissolved

volatile components, at the time of crystal growth (e.g., Lowenstern 1995; Danyushevsky et al. 2002; Metrich and Wallace 2008). However, after entrapment, the pressure inside of melt inclusions commonly decreases as a result of both crystallization along the melt-host interface and the greater thermal contraction of the melt compared with the host mineral (Roedder 1979; Anderson 1974; Lowenstern 1995). In addition, post-entrapment loss of H by diffusion through the host mineral can also contribute to the pressure decrease (Bucholz et al. 2013). The decrease in pressure leads to formation of a vapor bubble in the melt inclusion, and such bubbles are commonly referred to as shrinkage bubbles because of the process that forms them (e.g., Roedder 1984). Because the solubility of CO₂ in silicate melt is much lower than that of H₂O, resulting in a relatively high vapor-melt partition coefficient for CO₂, formation of a shrinkage bubble can strongly deplete the coexisting melt of dissolved CO₂ that was present at the time of entrapment.

For olivine-hosted melt inclusions, a decrease in temperature of 100 °C is estimated to create a shrinkage bubble that is 0.9

* E-mail: pwallace@uoregon.edu

† Present Address: BP America, Inc., Houston, Texas 77079, U.S.A.

‡ Special collection papers can be found on GSW at <http://ammin.geoscienceworld.org/site/misc/specialissuelist.xhtml>.

to 1.6 vol% of the inclusion (Anderson and Brown 1993; Riker 2005; Ruscitto et al. 2011). These estimates include both the effect of melt contraction due to cooling and the volume loss resulting from post-entrapment crystallization of olivine on inclusion walls. Further expansion of the shrinkage bubble occurs between eruption and quenching as the melt continues to contract down to the glass transition temperature, but this happens over such a short timescale that little to no additional volatiles are likely to diffuse from the melt to the bubble (Anderson and Brown 1993).

Determining original CO₂ contents for melt inclusions with shrinkage bubbles requires adding the mass of CO₂ in the bubble back into the inclusion. In addition to the experimental method described here, this has been done by estimating the CO₂ contents of bubbles (Anderson and Brown 1993; Riker 2005; Shaw et al. 2008; Steele-MacInnis et al. 2011) or by measurement of the CO₂ density in the bubble using micro-Raman spectroscopy (Esposito et al. 2011; Hartley et al. 2014; Moore et al. 2015). In their study of Kilauea Iki melt inclusions, Anderson and Brown (1993) estimated the amount of CO₂ that had been lost to shrinkage bubbles. They estimated that most bubble-bearing melt inclusions at Kilauea Iki contained pre-eruptive vapor bubbles that were ~0.5 vol% of the inclusion at their eruptive temperatures. The uncertainty in this method is knowing the size of the vapor bubble at the time of eruption, because cooling during eruption and quenching causes the vapor bubble to expand, but the timescale is sufficiently rapid that little additional CO₂ is likely to transfer from melt to bubble.

To quantitatively investigate the loss of CO₂ into shrinkage bubbles, we experimentally heated large melt inclusions in olivine from a Mauna Loa picrite to dissolve the vapor back into the melt. Our results demonstrate that 40–90% of the initial CO₂ that was dissolved in the melt inclusions was lost to the vapor bubble, with an average loss of 75%.

SAMPLES AND METHODS

The olivine used in this study are from Puu Wahi, a 910 yr B.P. line of scoria cones situated at ~3000 m elevation on the NE rift zone of Mauna Loa (Lockwood 1995). The olivine come from reticulite scoria and were naturally quenched to glass during eruption. Samples of this material were collected in 1997 by Wallace and A.T. Anderson. Melt inclusions in the olivine are commonly large (80–120 μm diameter), and all of the melt inclusions contain vapor bubbles that are ≤3 vol% of the inclusion. We analyzed one set of naturally quenched inclusions (n = 8) and performed heating experiments on a different set of inclusions (n = 12), all from the same scoria clast. As will be shown below, the olivine and melt inclusions mostly have fairly uniform compositions, making a comparison of heated vs. unheated inclusions useful for assessing how much CO₂ is in the vapor bubbles. An alternative methodology would have been to analyze individual melt inclusions by FTIR spectroscopy before and after heating, which can be done if the inclusions are not intersected during initial sample preparation (e.g., Massare et al. 2002). However, we chose not to use this approach because it does not allow the melt inclusion major element composition to be measured before heating, and therefore it is not possible to assess how post-entrapment crystallization has affected the volatile concentrations in the unheated inclusions. Furthermore, when doing heating experiments on thick wafers that still have MI fully enclosed, the chances of compromising inclusions by invisible cracks are very high.

Melt inclusions from other Puu Wahi clasts have been used for experiments on H diffusion through the olivine host (Gaetani et al. 2012) and for analysis of trace elements and Sr isotopes, which are remarkably diverse (Sobolev et al. 2011). The latter study reports olivine compositions of Fo_{82–89}, which is a much wider range than the olivine in the clast that we studied (Fo_{86.5–89.1}).

Individual crystals were heated using a Vernadsky Institute heating stage with controlled oxygen fugacity (Sobolev et al. 1980). All but one olivine were heated rapidly to 1420 °C for <10 min, which rehomogenized the vapor bubbles into the

melt. Such a high temperature is above the trapping temperatures (estimated below to be 1280 °C) but was required to get the vapor bubbles to rehomogenize quickly. After each inclusion was homogenized, power to the furnace was turned off to quench the inclusion to glass. However, even with the very rapid quenching that occurs in the Vernadsky stage, a vapor bubble formed in three of the melt inclusions (h4, h5, h7; see Table 1) during quench. Both unheated and heated inclusions were analyzed by FTIR spectroscopy and electron microprobe (Table 1).

To prepare the samples, the olivine host crystals were mounted on glass slides using acetone-soluble, thermal-setting cement and ground into doubly polished wafers with two parallel sides. The thickness of each melt inclusion was measured by mounting the edge of the doubly polished olivine wafer to a needle using epoxy and immersing the wafer into a cylindrical glass well filled with refractive index liquid (n = 1.657). This allows the crystal to be rotated and viewed parallel to the flat dimension under a microscope with a calibrated eyepiece, thereby allowing a direct measurement of the thickness. These measurements have an accuracy of ±1 to ±3 μm, depending on how close the inclusion is to the edge of the wafer.

Infrared spectroscopy

Transmission infrared spectra of the melt inclusion glasses were obtained using a Nicolet Magna 560 Fourier transform infrared spectrometer interfaced with a Spectra-Tech Nic-Plan microscope at Texas A&M University. For each melt inclusion, three individual spectra were taken using an adjustable rectangular aperture. All spectra were acquired using a KBr beamsplitter and liquid-nitrogen-cooled HgCdTe (MCT) detector.

The quantitative procedures and band assignments described in Dixon et al. (1995) were followed for this work. Quantitative measurements of dissolved total H₂O and carbonate (CO₃²⁻) were determined using Beer's law:

$$c = \frac{M A}{\rho d \epsilon}$$

where *c* is the concentration (in weight fraction) of the absorbing species, *M* is the molecular weight (18.02 for total H₂O; 44.00 for CO₂), *A* is the absorbance intensity of the band of interest, *ρ* is the room-temperature density of the glass, *d* is the thickness, and *ε* is the molar absorption coefficient.

Total dissolved H₂O was measured using the intensity of the broad, asymmetric band centered at 3530 cm⁻¹, which corresponds to the fundamental OH-stretching vibration. The absorbance intensity (peak height) was measured graphically from printed spectra, and the total H₂O concentration was calculated using an absorption coefficient of 63 ± 3 L/(mol·cm) (Dixon et al. 1995). Precision of the H₂O analyses is about ±5%.

Dissolved carbonate was measured from the absorbances of the bands at 1515 and 1430 cm⁻¹, which correspond to antisymmetric stretching of distorted carbonate groups (Fine and Stolper 1986; Dixon et al. 1995). Because the shape of the background in the region of the carbonate doublet is complex, absorbance intensities for the 1515 and 1430 cm⁻¹ bands were measured after subtraction of a reference spectrum for a decarbonated basaltic glass so as to achieve a relatively flat background (Dixon et al. 1995). The molar absorptivity for carbon dissolved as carbonate in basaltic glasses is compositionally dependent (Dixon and Pan 1995). Dissolved carbonate contents (reported in Table 1 and hereafter as the equivalent amount of CO₂, in parts per million) were determined using molar absorption coefficients of 353 ± 4 L/(mol·cm) (for unheated inclusions) and 360 ± 7 L/(mol·cm) (for heated inclusions), calculated from the average compositions of the glasses and the equation reported by Dixon and Pan (1995). Precision of the carbonate analyses is about ±20%.

One experimentally heated melt inclusion (PW_h1) had CO₂ below the detection limit (~25 ppm) and was quite anomalous in this regard compared to the other heated inclusions. This melt inclusion also had a very low S content. We do not consider this inclusion further in our analysis because of the likelihood that it formed originally at anomalously low pressure compared to the other inclusions.

Electron microprobe

Major elements and S were analyzed in all glasses with a Cameca SX-50 electron microprobe at Texas A&M University using mineral and glass standards. Analytical accuracy was assessed by analysis of U.S. National Museum glass standard VG-2. Sulfur was analyzed using an anhydrite standard, 60 s on-peak counting time, and a SKα wavelength offset measured on pyrite, which corresponds approximately to the S^{+/}S ratio expected for a basaltic glass equilibrated at the FMQ oxygen buffer (Wallace and Carmichael 1994). Analyses of glass standard VG-2 using this procedure yielded a S concentration of 0.137 ± 0.006 wt% (n = 11), similar to the value reported by Dixon et al. (1991) and Dixon and Clague

TABLE 1a. Compositional data for unheated melt inclusions

Inclusion	Unheated					PC_11	PC_21	PC_31	Avg. Corr.
	k97_17_11	k97_17_21	k97_17_31	k97_17_41	k97_17_51				
SiO ₂	52.81	52.40	52.59	53.08	52.39	52.35	51.71	52.48	50.71
TiO ₂	2.12	2.23	2.51	2.07	2.63	2.04	2.20	2.18	2.02
Al ₂ O ₃	13.81	13.98	13.77	14.01	14.02	13.79	13.44	13.73	12.44
FeO ^T	8.72	8.87	9.44	9.05	9.06	9.44	9.56	9.06	10.66
MnO	0.14	0.13	0.13	0.13	0.14	0.15	0.14	0.14	0.13
MgO	8.06	8.39	8.33	8.19	8.25	8.42	8.22	8.50	11.51
CaO	10.56	10.69	10.19	10.65	10.04	10.23	10.49	10.60	9.39
Na ₂ O	2.29	2.29	2.45	2.33	2.49	2.35	2.18	2.28	2.10
K ₂ O	0.46	0.44	0.46	0.29	0.68	0.42	0.49	0.39	0.41
P ₂ O ₅	0.29	0.26	0.28	0.19	0.29	0.27	0.30	0.29	0.24
S	0.125	0.137	0.064	0.096	0.131	0.140	0.124	0.107	0.10
H ₂ O	0.36	0.35	0.36	0.36	0.38	0.32	0.38	0.35	0.32
CO ₂	60	175	78	89	58	113	163	42	88
Total	99.74	100.17	100.57	100.45	100.49	99.92	99.22	100.12	100.00
Host Fo	88.0	88.2	88.1	88.2	88.5	88.0	87.7	88.2	88.1
H ₂ O corr.	0.33	0.32	0.33	0.33	0.34	0.29	0.34	0.32	
CO ₂ corr.	54	158	71	80	52	102	147	38	
P _{sat} (bars)	129	353	166	185	125	230	330	94	
Xv CO ₂	0.91	0.97	0.93	0.94	0.90	0.96	0.96	0.88	
CO ₂ restored	251	705	330	366	243	465	657	178	

Notes: All concentrations are in wt%, except for CO₂ and CO₂ restored, which are in parts per million. Olivine host composition is given in mol% forsterite. Column labelled Avg. Corr. is the average of unheated melt inclusions after correction for PEC and Fe loss. H₂O corr. and CO₂ corr. are values for each inclusion corrected for PEC and Fe loss. P_{sat} is vapor saturation pressure calculated using VolatileCalc. Xv CO₂ is mole fraction CO₂ in the vapor phase. CO₂ restored is based on estimated pre-eruption bubble volume of 1.25 vol% for each inclusion. See text for details.

TABLE 1b. Compositional data for heated melt inclusions

Inclusion	Heated											
	PW_h1	PW-h3A	PW_h3B	PW_h4	PW_h5	PW_h6	PW_h7	PW_h8	PW_h9	PW_h10	PW_h11	PW_h12
SiO ₂	49.95	49.61	49.13	51.01	50.04	51.16	50.08	49.01	49.55	49.74	48.29	49.12
TiO ₂	1.96	1.45	1.40	1.35	1.59	1.63	1.56	1.23	1.51	1.43	1.50	1.62
Al ₂ O ₃	10.90	9.52	9.49	10.40	10.14	10.61	10.46	9.14	10.34	9.98	10.22	10.22
FeO ^T	9.60	11.27	11.00	10.95	9.71	9.97	9.46	10.47	9.96	9.80	10.71	9.77
MnO	0.13	0.16	0.15	0.17	0.14	0.16	0.17	0.16	0.13	0.16	0.14	0.15
MgO	16.00	19.14	19.89	17.00	18.34	17.87	18.11	21.33	20.12	19.04	18.73	18.78
CaO	8.06	7.62	7.53	8.14	7.80	8.24	7.99	7.10	7.60	7.73	8.64	7.86
Na ₂ O	1.82	1.42	1.55	1.36	1.71	1.60	1.71	1.47	1.67	1.60	1.39	1.62
K ₂ O	0.34	0.27	0.28	0.24	0.25	0.25	0.26	0.29	0.30	0.24	0.20	0.25
P ₂ O ₅	0.23	0.25	0.19	0.20	0.21	0.20	0.20	0.20	0.25	0.16	0.17	0.20
S	0.009	0.099	0.094	0.070	0.045	0.079	0.049	0.075	0.132	0.024	0.113	0.086
H ₂ O	0.23	0.17	0.20	0.22	0.22	0.22	0.23	0.21	0.24	0.21	0.22	0.22
CO ₂	n.d.	278	370	207	210	230	201	159	340	162	282	294
Total	99.22	100.99	100.88	101.08	100.19	101.99	100.26	100.66	101.80	100.10	100.32	99.89
Host Fo	87.9	87.9	87.7	86.5	88.5	88.4	88.4	88.0	89.1	88.5	87.6	88.7
T _{heat}	1390	1420	1420	1420	1420	1420	1420	1420	1420	1420	1420	1400
Bubble				yes	yes	yes	yes					
H ₂ O corr.	0.26	0.23	0.27	0.31	0.28	0.28	0.30	0.29	0.29	0.30	0.31	0.29
CO ₂ corr.	n.d.	361	505	286	276	298	263	224	422	234	403	386
P _{sat} (bars)		776	1073	623	601	647	574	491	905	513	867	830
Xv CO ₂		0.99	0.99	0.98	0.99	0.99	0.98	0.98	0.99	0.98	0.99	0.99

Notes: T_{heat} is the temperature of experimental heating. Bubble indicates the inclusions in which a bubble re-formed on quenching.

(2001). The values reported in Table 1 are the averages of analyses of 3 spots on each melt inclusion. One standard deviation uncertainties based on replicate analyses are equal to the following amounts, in wt%: SiO₂ (0.17), TiO₂ (0.08), Al₂O₃ (0.08), FeO (0.15), MnO (0.02), MgO (0.06), CaO (0.10), Na₂O (0.06), K₂O (0.01), P₂O₅ (0.02), and S (0.008).

RESULTS

Photomicrographs of unheated and heated melt inclusions are shown in Figure 1. As described above, temperatures well above the original trapping temperature were required to get the vapor bubbles to rehomogenize quickly. It is likely that using longer heating times would have yielded lower homogenization temperatures because it would have allowed dissolved volatile contents, particularly slowly diffusing CO₂, to reach equilibrium concentrations by diffusion throughout the inclusion, but the short times were needed to minimize any loss of H by diffusion through the olivine. In addition, the fact that the pre-experiment

bubble vol% values were small (≤ 3 vol%) and in a fairly narrow range and that the bubble in each inclusion homogenized at a similar temperature suggest that none of the bubbles were primary bubbles that had been heterogeneously trapped with melt (Roedder 1984). The presence of primary bubbles would likely have caused a larger range in bubble vol% values (e.g., Moore et al. 2015) and consequently, much more variable homogenization temperatures and/or inclusions that could not be rehomogenized.

The compositions of the unheated and heated melt inclusions are shown on a diagram of FeO^T vs. MgO in Figure 2. The unheated melt inclusions are relatively uniform in composition. The host olivine compositions are also relatively uniform, with average Fo contents of 88.1 ± 0.2 in the unheated inclusions and 88.1 ± 0.7 in the heated inclusions. Assuming an olivine-melt K_d value of 0.3 (Roeder and Emslie 1970) and FeO/FeO^T of 0.85 (approximately FMQ), the analyzed compositions of the unheated inclusions are

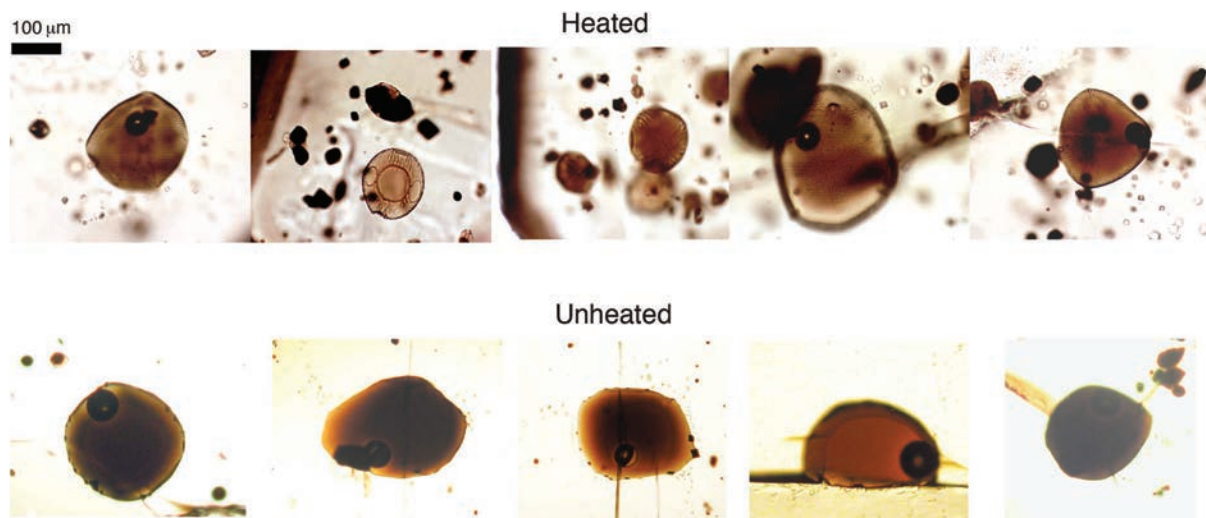


FIGURE 1. Photomicrographs of unheated and heated melt inclusions analyzed in this study. A 100 μm scale bar is shown at upper left. Note that some heated melt inclusions have a vapor bubble that appeared during quenching. All original vapor bubbles in the heated melt inclusions rehomogenized during the high-temperature heating experiment. (Color online.)

predicted to be in equilibrium with Fo_{86.4} olivine. This is an indication that the melt inclusions were affected by post-entrapment crystallization (PEC). Addition of equilibrium olivine in 0.1 wt% increments requires ~4% olivine added to restore the melt inclusion compositions to equilibrium with Fo_{88.1} olivine. Also shown in Figure 2 are the compositions of submarine glasses from the SW rift zone of Mauna Loa (Garcia et al. 1995) and whole rock and matrix glass separates for the 1852 and 1868 subaerial picritic eruptions on Mauna Loa (Rhodes 1995). The bulk rock picrite analyses show the effects of variable olivine accumulation and thus plot along an olivine control line. The fact that the PEC-corrected, unheated melt inclusion compositions fall below the trend shown for the picrite data suggests that the inclusions were affected by Fe diffusive loss (Danyushevsky et al. 2000), which also causes the true extent of PEC to be greater than calculated above for the case of no Fe loss. Correction for the effects of both Fe loss and PEC for the unheated melt inclusions yields an average initial melt inclusion composition with 11.7 wt% MgO and 10.8 wt% FeO^T and an average PEC estimate of 9.6 wt% olivine.

The analyzed compositions of the heated melt inclusions show much higher MgO (16–21.3 wt%) and slightly higher FeO^T (9.5–11.3 wt%) than the unheated inclusions. This makes them in equilibrium with Fo_{92.8} olivine, much higher than the actual host values. This is an indication that the experimental temperatures were above the original trapping temperatures, resulting in large amounts of olivine dissolution from the walls of the inclusions during the heating experiment. To correct the H₂O and CO₂ contents of the heated inclusions to be comparable to the corrected values for the unheated inclusions, we used elements that are incompatible in olivine (Ti, Al, Ca, K, P). We used the concentrations of these elements in each heated melt inclusion and the concentration in the average PEC and Fe-loss corrected composition for the unheated inclusions to calculate the excess olivine dissolved from the inclusion-host interface during the experimental heating according to the relationship:

$$\text{wt\% element in original trapped melt} \div \text{wt\% element, measured} = 1 + \text{wt. fraction excess olivine}$$

The results indicate that 22–43 wt% excess olivine (relative to the initial mass of melt) was dissolved during the experiments. This means that the concentrations of CO₂ and H₂O in the heated melt inclusions were diluted by the large amount of dissolved olivine caused by the overheating. We have corrected the concentrations using the equation above and the values for excess olivine dissolved for each heated inclusion calculated from the Ti, Al, Ca, K, and P data. It should be noted, however, that there can be significant heterogeneity in minor and trace

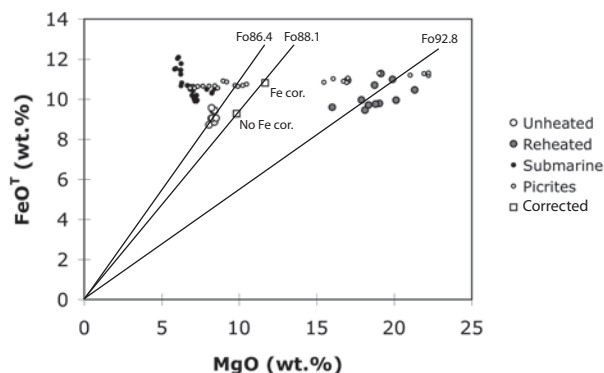


FIGURE 2. FeO^T vs. MgO for unheated and heated melt inclusions. The average composition of the unheated melt inclusions after correction for post-entrapment crystallization, with and without the effects of Fe diffusive loss, are shown as open squares. Diagonal lines show equilibrium values with various olivine compositions, as labeled. Shown for comparison are the compositions of submarine glasses from the SW rift zone of Mauna Loa (Garcia et al. 1995) and whole rock and matrix glass separates for the 1852 and 1868 subaerial picritic eruptions on Mauna Loa (Rhodes 1995).

elements within Hawaiian melt inclusions from a given sample (e.g., Sides et al. 2014), and this causes additional uncertainty in our calculation of excess olivine dissolved.

Even before accounting for the dilution effect caused by olivine dissolution, it is evident that the CO₂ concentrations (as measured) in the heated inclusions are significantly greater than those in the unheated inclusions (Table 1). After recalculation, as described above, to correct for the dilution effect, the CO₂ contents of the heated inclusions are 224–505 ppm ($n = 11$), much higher than the CO₂ contents of the naturally quenched inclusions (38–158 ppm; $n = 8$), all of which contain shrinkage bubbles (Fig. 3). The three melt inclusions in which shrinkage bubbles re-formed during quenching are at the lower end of the range of CO₂ values, but other bubble-free inclusions have similar and even lower values. The fact that vapor bubbles sometimes re-

formed is probably caused by the large difference between the peak heating temperature and the glass transition temperature, which results in extensive melt contraction relative to the olivine host during experimental quenching. This causes pressure to drop precipitously in a bubble-free melt inclusion (e.g., Lowenstern 1995). Therefore, even though the heated melt inclusions had dissolved substantial excess olivine and were therefore not vapor saturated at the beginning of quenching, the melt contraction and consequent large pressure drop would be sufficient to cause a vapor bubble to form. However, the experimental quenching time is rapid enough that very little CO₂ should diffuse into the bubble from the surrounding melt.

Dissolved H₂O contents of the melt inclusions, both heated and unheated, are very uniform (0.32 ± 0.02 wt% for unheated, 0.29 ± 0.02 wt% for heated, after correction for dilution effect). This indicates that minimal to no diffusive loss of H₂O occurred during the short heating time (e.g., Gaetani et al. 2012), despite the very high experimental temperatures. The slight difference between the two groups could be caused by uncertainties in the correction procedures. Our results demonstrate that substantial CO₂ is lost to shrinkage bubbles that form post-entrapment. A comparison of the average CO₂ content of heated inclusions (330 ± 90 ppm) and unheated inclusions (90 ± 50 ppm) indicates that 40–90% of the initial CO₂ that was dissolved in the melt inclusions was lost to shrinkage bubbles, with an average loss of 75%. These results are comparable to values estimated using micro-Raman spectroscopy on Solchiaro (Italy), Kilauea, and Laki (Iceland) melt inclusions (Esposito et al. 2011; Moore et al. 2015; Hartley et al. 2014).

Based on our results, it is clear that accurate pressures of trapping cannot be determined unless the CO₂ in shrinkage bubbles has been quantified. Pressures of melt inclusion entrapment calculated using the H₂O and CO₂ data for the corrected, heated inclusions range from 0.5 to 1.1 kbar (Fig. 4; pressures calculated using VolatileCalc; Newman and Lowenstern 2002). For comparison, pressures calculated for the unheated samples are 0.09 to 0.35 kbar. The H₂O and CO₂ variations in the heated inclusions are consistent with a degassing path (either closed- or open-system), which follows a vertical trajectory on a diagram of CO₂ vs. H₂O for melts with low H₂O concentration. This conclusion holds true even if the three melt inclusions that had bubbles re-form on quench are excluded. These results suggest that the olivine from a single scoria clast crystallized over a range of depths (~1.8–3.9 km for a crustal density of 2800 kg/m³), trapping variably degassed melts. This does not require that the olivine crystallized during closed-system ascent of a single batch of magma, as it is possible that they were pre-existing crystals, originally formed at various depths, that were entrained by rising melts. However, the narrow range of host olivine and melt inclusion compositions for the clast that we studied implies a close relationship or similar origin for the olivine.

Computational methods for assessing CO₂ lost to shrinkage bubbles

In the absence of experimental heating studies or direct measurement of CO₂ density in shrinkage bubbles by micro-Raman spectroscopy (Esposito et al. 2011; Hartley et al. 2014; Moore et al. 2015), it is possible to estimate the amount of CO₂

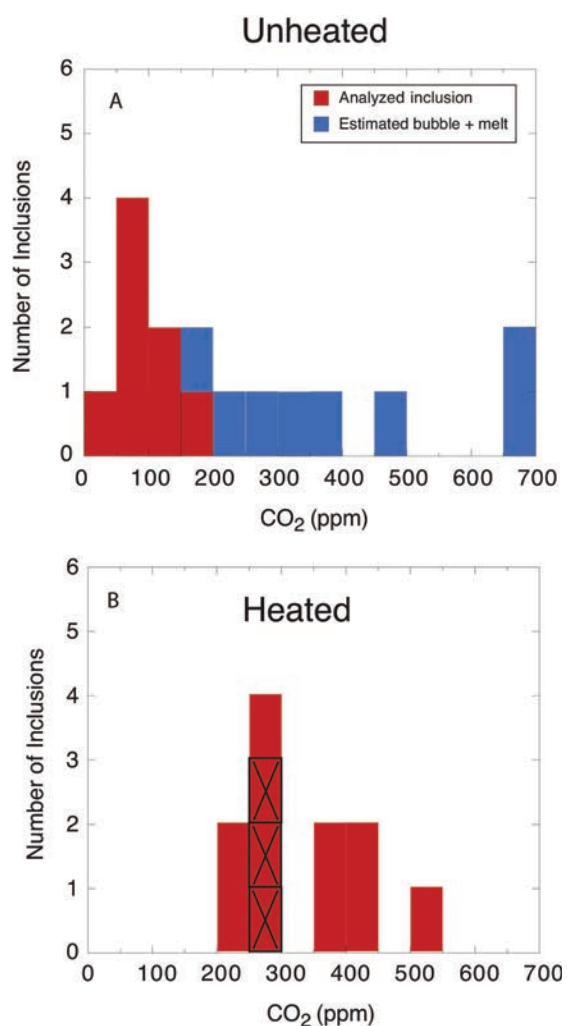


FIGURE 3. Histograms comparing CO₂ contents of (a) unheated and (b) heated melt inclusions, after correction to compositions in equilibrium with Fo_{88.1} olivine, as described in the text. Also shown in a are estimated CO₂ contents of the unheated inclusions calculated by assuming a 1.25 vol% pre-eruptive bubble in each inclusion. The three inclusions in b in which bubbles re-formed during quenching are marked with an X. (Color online.)

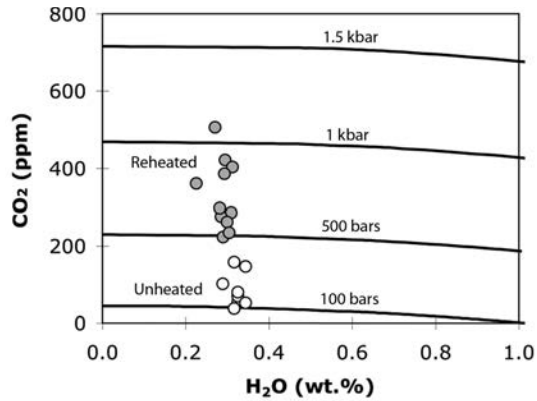


FIGURE 4. H₂O and CO₂ concentrations of unheated and heated melt inclusions after correction to compositions in equilibrium with Fo_{88.1} olivine, as described in the text. Vapor saturation isobars are calculated using VolatileCalc for a basaltic melt at 1280 °C.

that is in the bubbles. In this section we evaluate the accuracy of such estimates based on a comparison with our experimental results. It is important to note, however, that carbonate mineral phases have been detected on the walls of bubbles in some melt inclusions (Kamenetsky et al. 2001, 2002, 2007; Moore et al. 2015). Because the C in these carbonates is probably derived from CO₂ in the vapor bubble, the computational methods for estimating CO₂ lost to vapor bubbles may be accurate for melt inclusions that contain carbonates. In addition to carbonates in vapor bubbles, anomalously high C contents have been documented at the inclusion-host interface in some melt inclusions analyzed by SIMS using depth profiling (i.e., inclusions that were not exposed prior to analysis; Esposito et al. 2014). This could indicate that a thin film of CO₂-rich gas or carbonates is present in cracks along the inclusion-host interface as a result of differential shrinking of the melt and host crystal during quenching. Because experimental heating and homogenization are able to fully redissolve all of the CO₂ that was originally present in a melt inclusion at trapping (as long as the heating time is sufficient to redissolve any carbonate mineral phases), our results are valuable for testing the usefulness of computational methods used to infer original CO₂ contents.

As discussed previously, the major uncertainty in computational methods is knowing the size of the vapor bubble at the time of eruption, because cooling during eruption and quenching causes the vapor bubble to expand, but the timescale is sufficiently rapid that little additional CO₂ is probably lost from melt to bubble. In their study of Kilauea Iki melt inclusions, Anderson and Brown (1993) estimated that most bubble-bearing melt inclusions contained pre-eruptive gas bubbles of 0.5 vol% of the inclusion at their eruptive temperatures. Riker (2005) used phase equilibrium calculations together with volume and thermal expansion data for silicate melts and olivine to estimate a relationship for Mauna Loa tholeiitic melts describing the vol% bubble formed due to cooling and post-entrapment crystallization as a function of the difference between the trapping and pre-eruption temperatures. The resulting equation was:

$$\text{Bubble vol\%} = 0.0162 \Delta T$$

where $\Delta T = T_{\text{trapping}} - T_{\text{pre-eruption}}$. For the Puu Wahi melt inclusions, we estimate trapping and eruption temperatures using the experimentally calibrated thermometer of Montierth et al. (1995) based on melt MgO content. For the unheated inclusions, the composition corrected for effects of PEC and Fe loss has 11.7 wt% MgO, yielding a trapping temperature of 1280 °C. The temperature at the time of eruption can be estimated using the actual analyzed glass MgO values of the unheated inclusions, yielding a temperature of 1203 °C. For ΔT of 77 °C, we calculate that the pre-eruption bubble size for the Puu Wahi melt inclusions would have been 1.25 vol% using the Riker (2005) relationship.

Using this value for the pre-eruption bubble volume, we estimate how much CO₂ the vapor bubbles would have contained just prior to eruption. By adding this estimated mass of CO₂ back into each inclusion, we can estimate the concentration that the melt would have had at the time of trapping. To do this for each inclusion, we used the VolatileCalc program (Newman and Lowenstern 2002) to estimate the pressure of the inclusion and the mol% CO₂ in the vapor bubble at the pre-eruption temperature using the dissolved concentrations of H₂O and CO₂, and we used the Redlich-Kwong equation of state to determine the molar volume of CO₂ in the vapor bubble. In the Redlich-Kwong calculations, we ignored the effect of H₂O on the P - V - T properties of the mixed-volatile vapor phase because the vapor is nearly pure CO₂ (see Table 1). The results are given in Table 1 and shown in Figure 3 for comparison with the heated inclusions. The assumption of a 1.25 vol% pre-eruption bubble results in an estimated loss of 75% CO₂ to the shrinkage bubble, which agrees well with the percentage loss values that we estimate by comparing the CO₂ in the heated inclusions with those of the unheated inclusions.

As a further test, we created a forward model of the relationship between bubble vol% and the fraction of CO₂ lost to a bubble for a melt starting with 0.3 wt% H₂O and 340 ppm CO₂, the average of the heated melt inclusions (Fig. 5). The model uses a closed-system degassing calculation from VolatileCalc to simulate the effect of post-entrapment decompression in a melt inclusion. The use of VolatileCalc in this regard is a simplification because in a melt inclusion, the decompression occurs due to cooling-induced crystallization and melt contraction whereas in VolatileCalc the decompression occurs isothermally. Furthermore, in the natural system that we are simulating (Puu Wahi melt inclusions), post-entrapment crystallization of about 10 wt% olivine causes a small increase in dissolved volatiles in the inclusion, and we have ignored this effect as well. The calculations were done at 1200 °C, and for simplicity we assumed a constant melt density of 2800 kg/m³ (i.e., the calculations do not include the change in density of silicate melt, which is quite small over the pressure range considered) and we ignored the effect of the compressibility of olivine, which is also quite small. For each step of decreasing pressure in the closed-system degassing calculation, we calculated the mass and volume (using Redlich-Kwong, again ignoring the effect of H₂O on the P - V - T properties of the mixed volatile phase) of CO₂ that had exsolved from the melt and the mole fractions of CO₂ and H₂O in the vapor phase. For an assumed initial mass of a single phase melt inclusion at time of trapping, these values at each pressure step can be converted to vol% vapor bubble

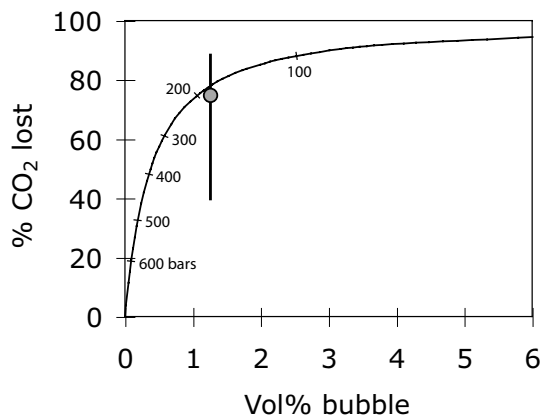


FIGURE 5. Relationship between vapor bubble vol% and the fraction of initial dissolved CO₂ lost to the bubble, calculated as described in the text. Tick marks along the curve show the internal pressure of the melt inclusion, in bars. The initial pressure at time of trapping (0.3 wt% H₂O, 340 ppm CO₂) is 740 bars. The data point shows the average estimated pre-eruptive bubble size for the Puu Wahi melt inclusions based on MgO content and calculated temperature (using Riker 2005) and the range in %CO₂ lost based on a comparison of heated and unheated inclusions. Vertical bar shows the range in percent lost (40–90%) values.

inside the inclusion. The results (Fig. 5) show that when the vapor bubble reaches 1.25 vol% of the inclusion, ~77% of the initial dissolved CO₂ has been lost to the bubble, and the internal pressure of the inclusion has dropped from 740 to ~200 bars. This agrees very well with the pre-eruptive bubble volume for the Puu Wahi melt inclusions calculated using Riker (2005) and the estimate of the fraction of initial CO₂ lost to the vapor bubbles based on our heating experiments.

Given this agreement, we conclude that the Riker (2005) method for estimating the pre-eruption bubble size for Hawaiian tholeiitic melts gives reliable results, in the absence of actual heating experiments or measurement of CO₂ densities in the inclusions by Raman spectroscopy. Based on the discussion above, we conclude that the fraction of the initial dissolved CO₂ in a melt inclusion that is lost to a shrinkage bubble (and any subsequently formed carbonates) is controlled by three factors: (1) the difference between the trapping and pre-eruption temperatures, which controls both the extent of differential shrinkage between melt and bubble and the extent of post-entrapment crystallization; (2) the trapping pressure; and (3) the initial H₂O and CO₂ contents of the melt, which determine the mole fraction of CO₂ in the vapor phase inside the bubble. In addition to these factors, Bucholz et al. (2013) have shown experimentally that diffusive H loss can also contribute to vapor bubble formation because of the increase in melt density caused by the loss of H₂O. Thus the extent of post-entrapment diffusive loss will also affect how much dissolved CO₂ is lost to a shrinkage bubble. One consequence of the third factor is that the effect of CO₂ loss to a shrinkage bubble is expected to be smaller for more H₂O-rich melt inclusions than those studied here because the vapor bubble in such inclusions will have lower mole fractions of CO₂ than the low-H₂O inclusions in our study. As a result, the predicted relationship shown in Figure 5 will change for melts with different H₂O values (cf. Steele-MacInnis et al. 2011).

Crystallization depths for Hawaiian picrites

Our results indicate that olivine crystallized at very shallow depths (~2 to 4 km) beneath the surface of Mauna Loa. Large fluid inclusions (≤100 μm in diameter) in some Puu Wahi olivine appear to contain relatively low-density CO₂ based on petrographic observations, consistent with the interpretation based on melt inclusions that olivine crystallized at low pressures. Such surprisingly low pressures of crystallization have also been inferred for olivine erupted in the 1959 Kilauea Iki picrite (mostly less than 4 km; Anderson and Brown 1993) and for abundant Fo_{88–90} olivine in the Keanakakoi ash deposits at Kilauea (Hart and Wallace 2000) based on computational methods for restoring CO₂. Eruptions of olivine-rich lava are relatively rare on the subaerial portions of both Kilauea and Mauna Loa but are more common on the submarine parts of both volcanoes. As has been proposed for Kilauea Iki (Helz 1987; Anderson and Brown 1993), the eruption of olivine-rich lava high on the NE rift zone of Mauna Loa probably resulted from magma following an unusual pathway to the surface, thus bypassing mixing and density filtering within the summit magma system.

Anderson (1995) demonstrated that exsolved CO₂ in picritic magmas plays an important role in making them buoyant enough to be eruptible. For Hawaiian picritic magma, an initial bulk CO₂ content of 0.3 wt% is sufficient to make the magma buoyant relative to degassed tholeiitic basaltic magma at pressures of 2 kbar or less, but at higher pressures the picritic magma is negatively buoyant because of the compressibility of the vapor phase. Thus Anderson (1995) concluded that the rarity of erupted picrites at Hawaii is likely because primitive magma typically enters the large summit reservoirs near their base, where the pressure is sufficiently high to cause the bulk density of parental magma to be greater than that of stored magma. Regardless of the mechanism, however, our new experimental results confirm that high-Mg olivine phenocrysts can crystallize at shallow depths beneath Hawaiian volcanoes.

IMPLICATIONS

Our results for experimentally heated melt inclusions indicate that 40–90% of the initial CO₂ that was dissolved in the melt inclusions at the time of trapping was lost to shrinkage bubbles, with an average loss of 75%. Calculated trapping pressures for heated melt inclusions (0.5–1.1 kbar) are significantly higher than the pressures calculated based only on the dissolved CO₂ in the naturally quenched inclusions (0.09–0.35 kbar). To accurately infer original pressures of crystallization and trapping for melt inclusions with shrinkage bubbles, the mass of CO₂ in the bubbles must be either measured or calculated. This can be done by rehomogenization experiments like those described here or through the application of micro-Raman spectroscopy. In the absence of either of these approaches, we have shown that the method of Riker (2005) for estimating pre-eruption bubble size is successful for estimating how much CO₂ is in shrinkage bubbles in melt inclusions from Hawaiian tholeiitic magmas. For other melt compositions, particularly those with higher H₂O contents, published olivine-melt thermometers could be used to calibrate similar relationships between post-entrapment cooling, extent of crystallization, and the vol% bubble that forms as a result. The effect of CO₂ loss to shrinkage bubbles is expected to be

smaller for more H₂O-rich melt inclusions than those studied here because the vapor bubble in such inclusions will have lower mole fractions of CO₂ than the low-H₂O inclusions in our study.

ACKNOWLEDGMENTS

We thank Matt Steele-MacInnis, Marie Edmonds, and Rosario Esposito for constructive reviews that helped improve the final manuscript. P.W. also gives special thanks to Fred Anderson for introducing him to Hawaiian volcanoes, melt inclusions, and the problem of shrinkage bubbles.

REFERENCES CITED

- Anderson, A.T. (1974) Evidence for a picritic, volatile-rich magma beneath Mt. Shasta, California. *Journal of Petrology*, 15, 243–267.
- (1995) CO₂ and the eruptibility of picrite and komatiite. *Lithos*, 34, 19–25.
- Anderson, A.T., and Brown, G.G. (1993) CO₂ contents and formation pressures of some Kilauean melt inclusions. *American Mineralogist*, 78, 794–803.
- Bucholz, C.E., Gaetani, G.A., Behn, M.D., and Shimizu, N. (2013) Post-entrapment modification of volatiles and oxygen fugacity in olivine-hosted melt inclusions. *Earth and Planetary Science Letters*, 374, 145–155.
- Danyushevsky, L.V., Della-Pasqua, F.N., and Sokolov, S. (2000) Re-equilibration of melt inclusions trapped by magnesian olivine phenocrysts from subduction-related magmas: petrological implications. *Contributions to Mineralogy and Petrology*, 138, 68–83.
- Danyushevsky, L.V., McNeill, A.W., and Sobolev, A.V. (2002) Experimental and petrological studies of melt inclusions in phenocrysts from mantle-derived magmas: an overview of techniques, advantages, and complications. *Chemical Geology*, 183, 5–24.
- Dixon, J.E., and Clague, D.A. (2001) Volatiles in basaltic glasses from Loihi Seamount: evidence for a relatively dry plume source. *Journal of Petrology*, 42, 627–654.
- Dixon, J.E., and Pan, V. (1995) Determination of the molar absorptivity of dissolved carbonate in basaltic glass. *American Mineralogist*, 80, 1339–1342.
- Dixon, J.E., Clague, D.A., and Stolper, E.M. (1991) Degassing history of water, sulfur, and carbon in submarine lavas from Kilauea Volcano, Hawaii. *Journal of Geology*, 99, 371–394.
- Dixon, J.E., Stolper, E.M., and Holloway, J.R. (1995) An experimental study of water and carbon dioxide solubilities in Mid-Ocean Ridge basaltic liquids. Part I: calibration and solubility models. *Journal of Petrology*, 36, 1607–1631.
- Esposito, R., Bodnar, R.J., Danyushevsky, L.V., de Vivo, B., Fedele, L., Hunter, J., Lima, A., and Shimizu, N. (2011) Volatile evolution of magma associated with the Solchiaro eruption in the Phlegrean Volcanic District (Italy). *Journal of Petrology*, 52, 2431–2460.
- Esposito, R., Hunter, J., Schiffbauer, J.D., Shimizu, N., and Bodnar, R.J. (2014) An assessment of the reliability of melt inclusions as recorders of the pre-eruptive volatile content of magmas. *American Mineralogist*, 99, 976–998.
- Fine, G., and Stolper, E. (1986) Carbon dioxide in basaltic glasses: concentrations and speciation. *Earth and Planetary Science Letters*, 76, 263–278.
- Gaetani, G.A., O'Leary, J.A., Shimizu, N., Bucholz, C.E., and Newville, M. (2012) Rapid reequilibration of H₂O and oxygen fugacity in olivine-hosted melt inclusions. *Geology*, 40, 915–918.
- Garcia, M.O., Hulsebosch, T.P., and Rhodes, J.M. (1995) Olivine-rich submarine basalts from the southwest rift zone of Mauna Loa Volcano: Implications for magmatic processes and geochemical evolution. In J.M. Rhodes and J.P. Lockwood, Eds., *Mauna Loa Revealed: Structure, Composition, History, and Hazards*, 92, 219–239. American Geophysical Union, Geophysical Monograph, Washington, D.C.
- Hart, D., and Wallace, P.J. (2000) Volatiles in melt inclusions from the Keanakakoi Ash Member, Kilauea Volcano: Implications for explosive Hawaiian eruptions. *Eos, Transactions American Geophysical Union*, 81, 1291.
- Hartley, M.E., MacLennan, J., Edmonds, M., and Thordarson, T. (2014) Reconstructing the deep CO₂ degassing behaviour of large basaltic fissure eruptions. *Earth and Planetary Science Letters*, 393, 120–131.
- Helz, R. (1987) Diverse olivine types in lava of the 1959 eruption of Kilauea volcano and their eruption dynamics. USGS Professional Paper, 1350, 691–722.
- Kamenetsky, V.S., Binns, R.A., Gemmill, J.B., Crawford, A.J., Mernagh, T.P., Maas, R., and Steele, D. (2001) Parental basaltic melts and fluids in eastern Manus backarc basin: Implications for hydrothermal mineralisation. *Earth and Planetary Science Letters*, 184, 685–702.
- Kamenetsky, V.S., Davidson, P., Mernagh, T.P., Crawford, A.J., Gemmill, J.B., Portnyagin, M.V., and Shinjo, R. (2002) Fluid bubbles in melt inclusions and pillow-rim glasses: high-temperature precursors to hydrothermal fluids? *Chemical Geology*, 183, 349–364.
- Kamenetsky, V.S., Pompilio, M., Metrich, N., Sobolev, A.V., Kuzmin, D.V., and Thomas, R. (2007) Arrival of extremely volatile-rich high-Mg magmas changes explosivity of Mount Etna. *Geology*, 35, 255–258.
- Lockwood, J.P. (1995) Mauna Loa eruptive history—The preliminary radiocarbon record. In J.M. Rhodes and J.P. Lockwood, Eds., *Mauna Loa Revealed: Structure, Composition, History, and Hazards*, 92, p. 81–94. American Geophysical Union, Geophysical Monograph, Washington, D.C.
- Lowenstern, J.B. (1995) Application of silicate-melt inclusions to the study of magmatic volatiles. In J.F.H. Thompson, Ed., *Magmas, Fluids and Ore Deposits*, 23, p. 71–100. Mineralogical Association of Canada, Short Course Series, Quebec.
- Massare, D., Metrich, N., and Clochiatti, R. (2002) High-temperature experiments on silicate melt inclusions in olivine at 1 atm: inference on temperatures of homogenization and H₂O concentrations. *Chemical Geology*, 183, 87–98.
- Metrich, N., and Wallace, P.J. (2008) Volatile abundances in basaltic magmas and their degassing paths tracked by melt inclusions. *Reviews in Mineralogy and Geochemistry*, 69, 363–402.
- Montieth, C., Johnston, A.D., and Cashman, K.V. (1995) An empirical glass-composition-based geothermometer for Mauna Loa lavas. In J.M. Rhodes and J.P. Lockwood, Eds., *Mauna Loa Revealed: Structure, Composition, History, and Hazards*, 92, p. 207–217. American Geophysical Union, Geophysical Monograph, Washington, D.C.
- Moore, L., Gazel, E., Tuohy, R., Lloyd, A., Esposito, R., Steele-MacInnis, M., Hauri, E.H., Wallace, P.J., Plank, T., and Bodnar, R.J. (2015) Bubbles matter: An assessment of the contribution of vapor bubbles to melt inclusion volatile budgets. *American Mineralogist*, 100, 806–823.
- Newman, S., and Lowenstern, J.B. (2002) VolatileCalc: a silicate melt-H₂O-CO₂ solution model written in Visual Basic Excel. *Computers in Geosciences*, 2, 597–604.
- Rhodes, J.M. (1995) The 1852 and 1868 Mauna Loa picrite eruptions: Clues to parental magma compositions and the magmatic plumbing system. In J.M. Rhodes and J.P. Lockwood, Eds., *Mauna Loa Revealed: Structure, Composition, History, and Hazards*, 92, p. 241–262. American Geophysical Union, Geophysical Monograph, Washington, D.C.
- Riker, J. (2005) The 1859 eruption of Mauna Loa Volcano, Hawaii: Controls on the development of long lava channels. Unpublished M.S. thesis, University of Oregon.
- Roedder, E. (1979) Origin and significance of magmatic inclusions. *Bulletin de Mineralogie*, 102, 467–510.
- (1984) Fluid Inclusions. *Reviews in Mineralogy*, 12, 646 p.
- Roeder, P.L., and Emslie, R.F. (1970) Olivine-liquid equilibrium. *Contributions to Mineralogy and Petrology*, 29, 275–289.
- Ruscitto, D.M., Wallace, P.J., and Kent, A.J.R. (2011) Revisiting the compositions and volatile contents of olivine-hosted melt inclusions from the Mount Shasta region: Implications for the formation of high-Mg andesites. *Contributions to Mineralogy and Petrology*, 162, 109–132.
- Shaw, A.M., Hauri, E.H., Fischer, T.P., Hilton, D.R., and Kelly, K.A. (2008) Hydrogen isotopes in Mariana arc melt inclusions: Implications for subduction dehydration and the deep-Earth water cycle. *Earth and Planetary Science Letters*, 275, 138–145.
- Sides, I., Edmonds, M., MacLennan, J., Houghton, B.F., Swanson, D.A., and Steele-MacInnis, M.J. (2014) Magma mixing and high fountaining during the 1959 Kilauea Iki eruption, Hawaii. *Earth and Planetary Science Letters*, 400, 102–112.
- Sobolev, A.V., Dmitriev, L.V., Barsukov, L.V., Nevzorov, V.L., and Slutskii, A.V. (1980) The formation conditions of the high-magnesium olivines from the monomineralic fraction of Luna 24 regolith. *Lunar and Planetary Science Conference, 11th*, Houston, Texas, Proceedings. Volume 1, 105–116. Pergamon Press, New York.
- Sobolev, A.V., Hofmann, A.W., Jochum, K.P., Kuzmin, D.V., and Stoll, B. (2011) A young source for the Hawaiian plume. *Nature*, 476, 434–437.
- Steele-MacInnis, M., Esposito, R., and Bodnar, R. J. (2011) Thermodynamic model for the effect of post-entrapment crystallization on the H₂O-CO₂ systematics of vapor-saturated, silicate melt inclusions. *Journal of Petrology*, 52, 2461–2482.
- Wallace, P.J., and Carmichael, I.S.E. (1994) Sulfur speciation in submarine basaltic glasses as determined by measurements of SK α X-ray wavelength shifts. *American Mineralogist*, 79, 161–167.

MANUSCRIPT RECEIVED APRIL 29, 2014

MANUSCRIPT ACCEPTED OCTOBER 29, 2014

MANUSCRIPT HANDLED BY ROSARIO ESPOSITO